ELSEVIER

Journal of Alloys and Compounds 388 (2005) 49–58

Journal of ALLOYS AND COMPOUNDS

www.elsevier.com/locate/jallcom

Pressure dependence of hydrogen-induced transformations in C15 Laves phase $DyFe_2$ studied by pressure differential scanning calorimetry

H.-W. Li[b], K. Ishikawa[a], K. Aoki[a,*]

[a] *Department of Materials Science, Kitami Institute of Technology, 165 Koen-cho, Kitami, Hokkaido 090-8507, Japan*
[b] *Graduate School of Kitami Institute of Technology, 165 Koen-cho, Kitami, Hokkaido 090-8507, Japan*

Received 9 June 2004; received in revised form 26 June 2004; accepted 26 June 2004

Abstract

By thermal analysis of $DyFe_2$: (1) hydrogen absorption; (2) hydrogen-induced amorphization (HIA); (3) the precipitation of BiF_3-type DyH_3; and (4) the decomposition of the remaining amorphous hydride occur exothermically with increasing temperature at 1.0 MPa H_2. T_p/T_m (the peak temperature/the melting temperature of $DyFe_2$) for hydrogen absorption, HIA, the precipitation of DyH_3 and the decomposition of the amorphous hydride are 0.28, 0.36, 0.43 and 0.48, respectively, which are closely related with kinetics of the transformations. The peak temperature T_p for HIA shows a large and negative pressure dependence, but that for the precipitation of DyH_3 shows a small and positive one. As a consequence of such pressure dependence, HIA overlaps with the precipitation of DyH_3 at 0.2 MPa H_2, while the crystalline hydride decomposes directly into α-Fe and DyH_3 at 0.1 MPa H_2. The activation energy E_A for hydrogen absorption, HIA, the precipitation of DyH_3 and the decomposition of the amorphous hydride are calculated to be 56, 75, 308 and 162 kJ/mol Dy, respectively, which are closely related with the mechanism of HIA. The mechanism of HIA is discussed on the basis of the experimental results.

Keywords: Hydrogen absorption; Amorphous; C15 Laves compound; Hydrogen-induced amorphization; Thermal analysis

1. Introduction

Amorphous alloys are mainly prepared by rapid quenching of molten alloys. On the other hand, it has been known that an amorphous hydride is prepared by hydrogenation of intermetallic compounds A_xB_{1-x} with specific crystal structures such as C15, $B8_2$, C23, $D0_{19}$ and $L1_2$ [1–11], which is called hydrogen-induced amorphization (HIA). Here, A and B are a hydride forming and a non-hydride forming metal, respectively. Among amorphizing compounds, structural changes in the C15 Laves compounds RFe_2 (R = rare earth metals) are particularly interesting, because a crystalline and an amorphous hydride are formed depending on the hydrogenation temperature [7]. More recently, it has been reported that HIA in both $TbFe_2$ and $ErFe_2$ occurs at a given hydrogen pressure or higher pressures [12–15], but that HIA in $CeFe_2$ does occur for every hydrogen pressure [14]. The reason why HIA occurs above a critical hydrogen pressure is still uncertain. It is useful and effective to examine conditions of HIA in order to make clear the reason why HIA occurs above a critical hydrogen pressure, which is closely related with the mechanism of HIA. In the present work, the hydrogen pressure dependence of structural changes in the C15 Laves phase $DyFe_2$ is investigated using a pressure differential scanning calorimeter (PDSC). Furthermore, the enthalpy change (ΔH) and the activation energy (E_A) for the thermal reactions are measured by PDSC. The mechanism of HIA in $DyFe_2$ is discussed on the basis of the experimental results.

2. Experimental

$DyFe_2$ was prepared using high purity metals, 99.9% Fe and 99.8% Dy, by arc melting in a purified argon atmosphere. The alloy ingot was homogenized at 1073 K for 1 week in an

* Corresponding author. Tel.: + 81-157-26-9452; fax: + 81-157-26-9452.
E-mail address: aokiky@mail.kitami-it.ac.jp (K. Aoki).

0925-8388/$ – see front matter © 2004 Elsevier B.V. All rights reserved.
doi:10.1016/j.jallcom.2004.06.072

evacuated quartz tube. After the homogenization, the ingot was crushed into 100 mesh in acetone to prevent oxidation and ignition. The powder sample was thermally analyzed using a pressure differential scanning calorimeter at the rates of 0.08, 0.17, 0.33 and 0.67 K/s in a hydrogen atmosphere of 0.1–5.0 MPa. To elucidate the origin of the thermal peaks, $DyFe_2$ was heated to typical stages in PDSC, followed by rapid cooling to room temperature. Subsequently, it was subjected to powder X-ray diffraction (XRD) and conventional DSC (Ar-DSC) heated at a rate of 0.67 K/s in a flowing argon atmosphere. Some samples were further examined in a transmission electron microscope (TEM). The thermal desorption spectrum (TDS) of hydrogen and the amount of desorbed hydrogen were measured by heating the sample at a rate of 2 K/s in an argon atmosphere by a hydrogen analyzer. The enthalpy change ΔH and the activation energy E_A for thermal reactions were calculated from the area of the exothermic peaks in the PDSC curves and by the Kissinger method, respectively.

3. Results

3.1. Structural changes of $DyFe_2$ heated in a hydrogen atmosphere

Fig. 1 shows the PDSC curves of $DyFe_2$ heated at rates of 0.08–0.67 K/s and at a hydrogen pressure of 0.1–5.0 MPa. Four exothermic peaks are mainly observed in these PDSC curves, but only three or two ones are also observed depending on the hydrogen pressure and the heating rate. Typical PDSC curves and the change of the hydrogen content (H/M) heated at the rate of 0.17 K/s are shown in Fig. 2. The broken line denotes the base line, while the arrow indicates the temperatures to which the samples were heated and then rapidly cooled.

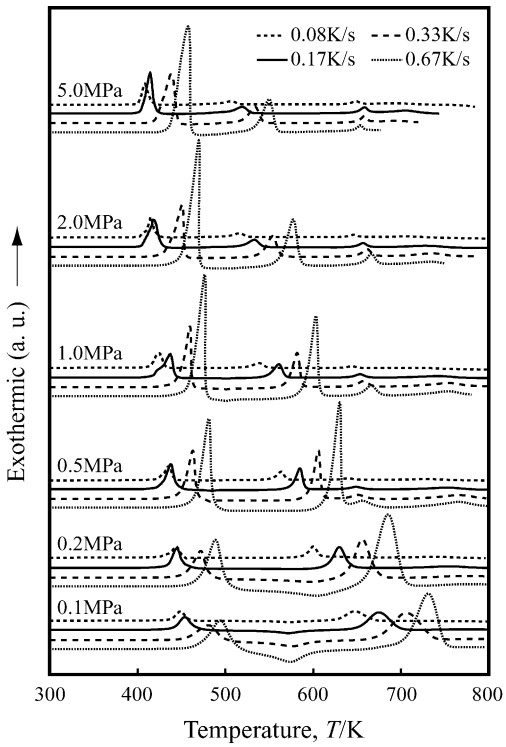

Fig. 1. PDSC curves of $DyFe_2$ heated at the rates of 0.08–0.67 K/s and at the hydrogen pressure of 0.1–5.0 MPa.

3.1.1. Structural changes of $DyFe_2$ heated in 1.0 MPa H_2

Four exothermic peaks are observed in the PDSC curve of $DyFe_2$ heated in 1.0 MPa H_2. The XRD patterns, TEM photographs and Ar-DSC curves of the $DyFe_2$ samples heated to above the respective exothermic peaks are shown in Figs. 3–5, respectively. The XRD pattern of the original sample indicates that this alloy consists of the C15 Laves phase [Fig. 3(1)]. The XRD pattern of the sample heated to above the first exothermic peak (460 K) shows Bragg peaks indexed

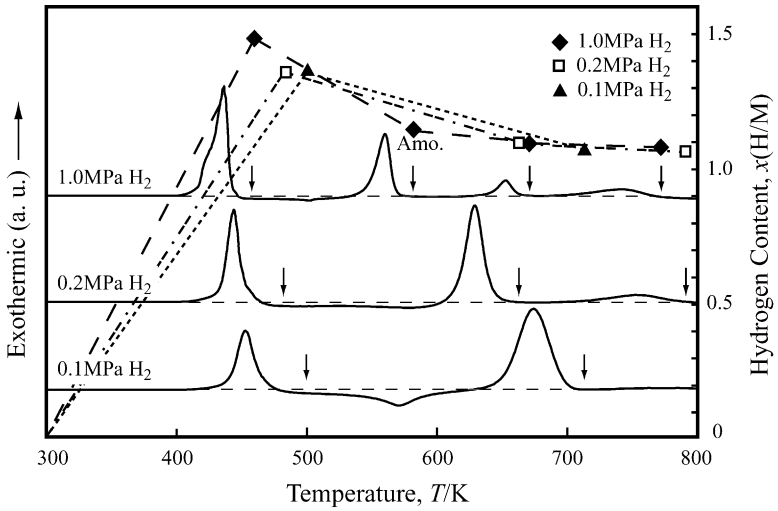

Fig. 2. Typical PDSC curves of $DyFe_2$ and the change in the hydrogen content (H/M) heated at the rate of 0.17 K/s.

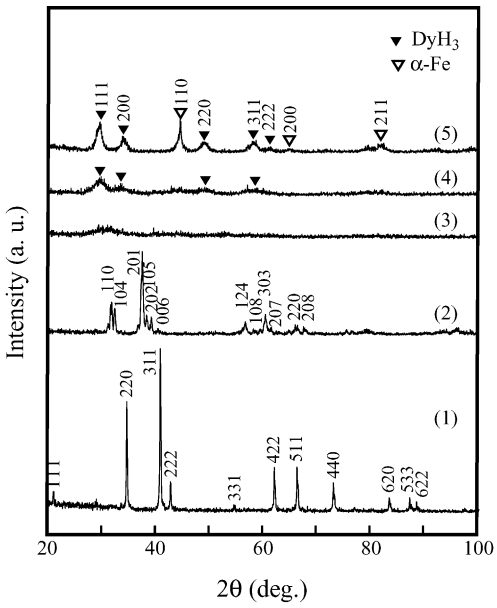

Fig. 3. XRD patterns of $DyFe_2$ heated to above respective stages of PDSC at the rate of 0.17 K/s in 1.0 MPa H_2. The original sample (1), the sample heated to above the first peak (460 K) (2), the second peak (583 K) (3), the third peak (673 K) (4), and the fourth peak (773 K) (5).

on the basis of a rhombohedral structure ($R\bar{3}m$) [Fig. 3(2)]. Its hydrogen content is 1.48 (H/M). The crystalline image is observed in the bright field TEM image for this sample [Fig. 4(a)] and the corresponding selected area diffraction pattern (SADP) shows a highly strained rhombohedral structure [Fig. 4(b)]. Furthermore, its Ar-DSC curve does not show any exothermic peak of crystallization [Fig. 5(1)]. Consequently, the first exothermic peak of PDSC is concluded to result from the formation of a crystalline hydride, i.e. crystalline c-$DyFe_2$ changes to c-$DyFe_2H_{4.4}$ at peak I. The Bragg peaks disappear and are replaced by a broad maximum in the sample heated to above the second exothermic peak (583 K) [Fig. 3(3)]. The hydrogen content of this sample is reduced to 1.13 (H/M). The bright field TEM image for this sample is featureless [Fig. 4(c)] and its SADP shows a broad halo characteristic of the amorphous state [Fig. 4(d)]. Furthermore, its Ar-DSC curve shows an exothermic peak of crystallization at around 900 K [Fig. 5(2)]. These experimental results imply that the sample heated to above the second exothermic peak of PDSC is amorphous. Consequently, the second exothermic peak of the PDSC curve results from the transformation from c-$DyFe_2H_{4.4}$ to a-$DyFe_2H_{3.4}$, i.e. hydrogen-induced amorphization. Broad and weak Bragg peaks of BiF_3-type DyH_3 appear overlapped with a broad maximum in the sample heated to above the third exothermic peak (673 K) [Fig. 3(4)]. Crystalline particles are embedded in the amorphous matrix in the bright field image of this sample [Fig. 4(e)] and its SADP shows Debye–Scherrer rings [Fig. 4(f)] of BiF_3-type DyH_3 overlapped with a broad halo. Furthermore, its Ar-DSC curve shows a broad exothermic peak at around 800–900 K, indicating survival of the amorphous hydride [Fig. 5(3)].

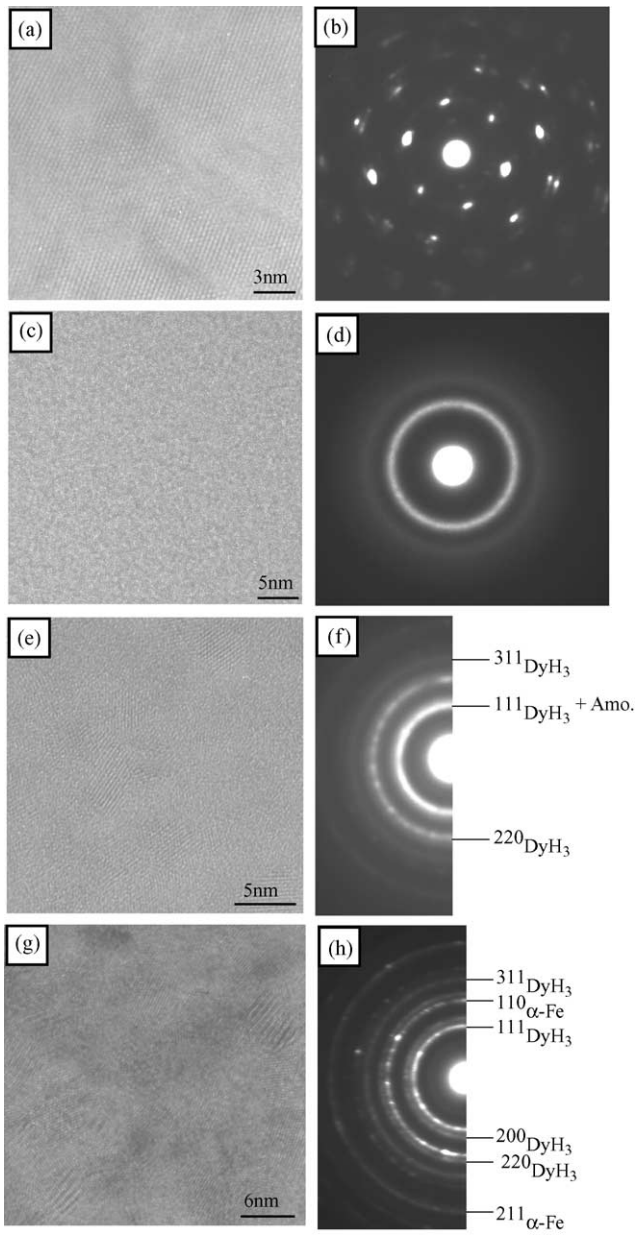

Fig. 4. Bright field images (a, c, e, g) and selected area diffraction patterns (b, d, f, h) of $DyFe_2$ heated to above respective stages of PDSC at a rate of 0.17 K/s in 1.0 MPa H_2. The sample heated to above the first peak (460 K) (a and b), the second peak (583 K) (c and d), the third peak (673 K) (e and f), and the fourth peak (773 K) (g and h).

From these experimental results, we can see that the third exothermic peak of PDSC results from the precipitation of BiF_3-type DyH_3 in the amorphous hydride. The crystal structure identification of the Dy hydride is discussed in Sections 3.3 and 4.1.

The XRD pattern of the sample heated to above the fourth exothermic peak (773 K) is indexed on the basis of α-Fe and BiF_3-type DyH_3 [Fig. 3(5)]. Dark particles can be observed in a bright-field TEM image [Fig. 4(g)] for this sample and its SADP shows the Debye–Scherrer rings indexed on the

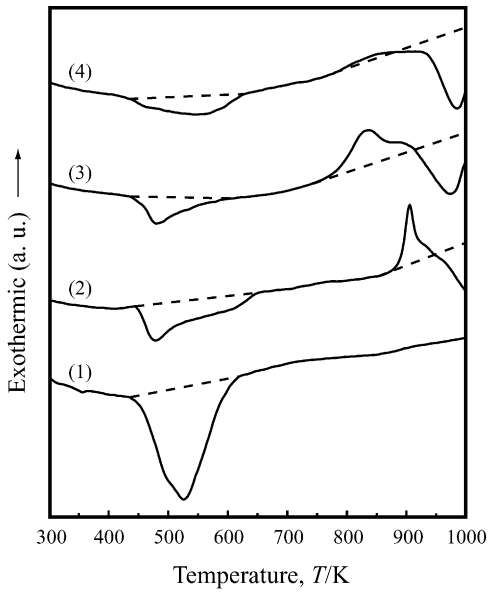

Fig. 5. Ar–DSC curves, heated at the rate of 0.67 K/s in an Ar atmosphere, for $DyFe_2$ after heating to above respective stages of PDSC at a rate of 0.17 K/s and in 1.0 MPa H_2. The sample heated to above the first peak (460 K) (1), the second peak (583 K) (2), the third peak (673 K) (3), and the fourth peak (773 K) (4).

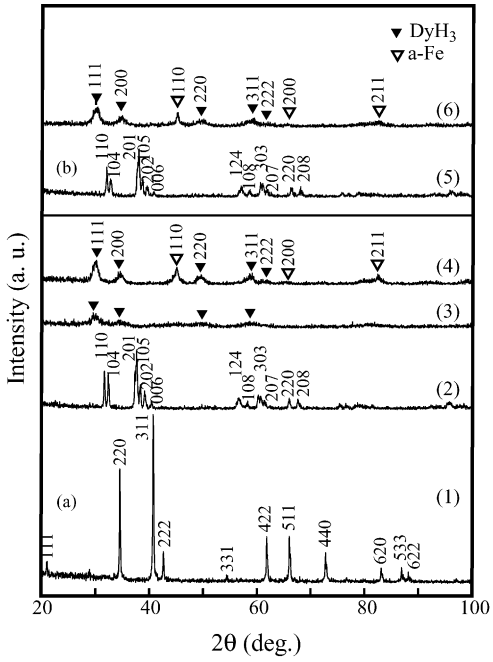

Fig. 6. XRD patterns of $DyFe_2$ heated to above respective stages of PDSC at the rate of 0.17 K/s in 0.2 MPa H_2 (a) and 0.1 MPa H_2 (b). The original sample (1), the sample heated to above the first peak (483 K) (2), the second peak (666 K) (3), the third peak (793 K) (4), the first peak (500 K) (5) and the second peak (714 K) (6).

basis of α-Fe and BiF_3-type DyH_3 [Fig. 4(h)]. Furthermore, its Ar-DSC curve does not show any exothermic peak of crystallization [Fig. 5(4)]. The hydrogen content of this sample is 1.08 (H/M), i.e. 3.24 (H/Dy). Consequently, the fourth exothermic peak of PDSC results from the decomposition of the remaining amorphous hydride into α-Fe and BiF_3-type DyH_3. The reaction sequence of $DyFe_2$ heated in 1.0 MPa H_2 is expressed as follows.

$$\text{c-DyFe}_2 \underset{\text{Peak I}}{\rightarrow} \text{c-DyFe}_2\text{H}_x \underset{\text{Peak II}}{\rightarrow} \text{a-DyFe}_2\text{H}_x$$
$$\underset{\text{Peak III}}{\rightarrow} \text{a-Dy}_{1-y}\text{Fe}_2\text{H}_x + \text{DyH}_3 \underset{\text{Peak IV}}{\rightarrow} \alpha\text{-Fe} + \text{DyH}_3$$

The reduced peak temperature (peak temperature/melting temperature of $DyFe_2$) T_p/T_m for hydrogen absorption, HIA, the precipitation of BiF_3-type DyH_3 and the decomposition of the amorphous hydride are 0.28, 0.36, 0.43 and 0. 48, respectively. These values are closely related with the diffusion of the metallic atoms as discussed later.

3.1.2. Structural changes of $DyFe_2$ heated in 0.2 MPa H_2

Three exothermic peaks are observed in the PDSC curve of $DyFe_2$ heated in 0.2 MPa H_2. The XRD patterns and Ar-DSC curves of the sample heated to above the exothermic peaks of PDSC are shown in Figs. 6(a) and 7(a), respectively. Comparing Fig. 3 with Fig. 6(a) and Fig. 5 with Fig. 7(a), we can see that the state of the samples heated to above the first, the second and the third exothermic peaks of PDSC heated in 0.2 MPa H_2 are c-$DyFe_2H_x$, a-$DyFe_2H_x$ + DyH_3 and α-Fe + DyH_3, respectively. That is, the first, the second and the third exothermic peaks result from the formation of a

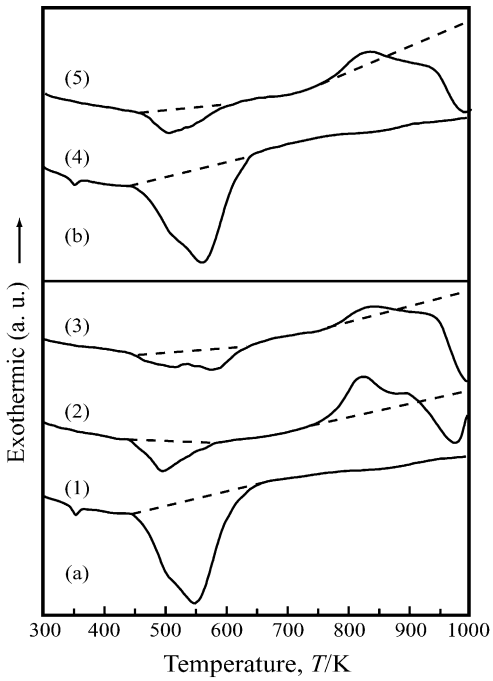

Fig. 7. Ar-DSC curves, heated at 0.67 K/s in an Ar atmosphere, for $DyFe_2$ after heating to above respective stages of PDSC at the rate of 0.17 K/s and in 0.2 MPa H_2 (a) and 0.1 MPa H_2 (b). The sample heated to above the first peak (483 K) (1), the second peak (666 K) (2), the third peak (793 K) (3), the first peak (500 K) (4) and the second peak (714 K) (5).

crystalline hydride, simultaneous occurrence of HIA and the precipitation of BiF_3-type DyH_3 and the decomposition of the remaining amorphous hydride into α-Fe and BiF_3-type DyH_3, respectively. The hydrogen content of the crystalline hydride is 1.36 (H/M). No single-phase amorphous hydride is formed under the present experimental conditions. The reaction sequence of $DyFe_2$ heated in 0.2 MPa H_2 is expressed as follows.

$$\text{c-DyFe}_2 \underset{\text{Peak I}}{\rightarrow} \text{c-DyFe}_2\text{H}_x \underset{\text{Peak II}}{\rightarrow} \text{a-Dy}_{1-y}\text{Fe}_2\text{H}_x + \text{DyH}_3 \underset{\text{Peak III}}{\rightarrow} \alpha\text{-Fe} + \text{DyH}_3$$

3.1.3. Structural changes of $DyFe_2$ heated in 0.1 MPa H_2

Two exothermic peaks are observed in the PDSC curve of $DyFe_2$ heated in 0.1 MPa H_2. The XRD patterns and Ar-DSC curves of the sample heated to above the exothermic peaks of PDSC are shown in Figs. 6(b) and 7(b), respectively. The first exothermic peak is due to the formation of a crystalline hydride in the same way as the other cases. The hydrogen content of the crystalline hydride is 1.36 (H/M), which is same as that of the sample heated in 0.2 MPa H_2. The XRD pattern of the sample heated to above the second exothermic peak (714 K) is indexed on the basis of α-Fe and BiF_3-type DyH_3.

Fig. 8 shows the lattice image in the bright field TEM image for the sample heated to above the second exothermic peak and its SADP shows Debye–Scherrer rings indexed on the basis of α-Fe and BiF_3-type DyH_3. Furthermore, its Ar-DSC curve does not show any exothermic peak of crystallization. Consequently, the second exothermic peak is due to the direct decomposition of c-$DyFe_2H_{4.1}$ into α-Fe + DyH_3. No amorphous hydride is detected under the present experimental conditions. The reaction sequence of $DyFe_2$ heated in 0.1 MPa is expressed as follows.

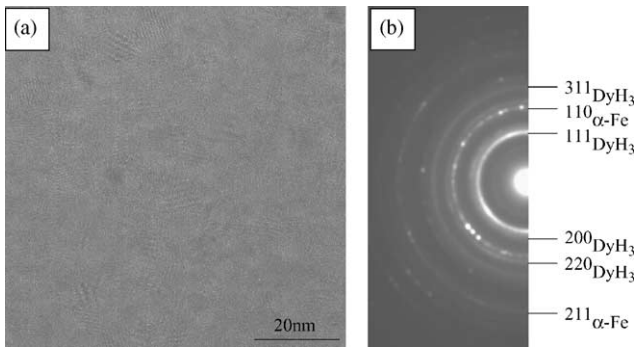

Fig. 8. TEM bright field image: (a) and SADP; (b) of $DyFe_2$ heated to 714 K at the rate of 0.17 K/s in 0.1 MPa H_2.

$$\text{c-DyFe}_2 \underset{\text{Peak I}}{\rightarrow} \text{c-DyFe}_2\text{H}_x \underset{\text{Peak II}}{\rightarrow} \alpha\text{-Fe} + \text{DyH}_3$$

Thus, all of the first exothermic peaks are due to hydrogen absorption in the crystalline state. On the other hand, the second exothermic peaks result from HIA, HIA+ the precipitation of BiF_3-type DyH_3 and the direct decomposition of the crystalline hydride into α-Fe + DyH_3 with decreasing hydrogen pressure. It is worth noticing that HIA occurs only at 0.2 MPa H_2 or even higher pressures.

3.2. The relation between the hydrogen pressure and the peak temperature T_p for thermal reactions

Fig. 9 shows the relation between the hydrogen pressure and the peak temperatures T_p for the thermal reactions for two heating rates of 0.17 K/s (the solid symbol and the solid line) and 0.33 K/s (the open symbol and the broken line).

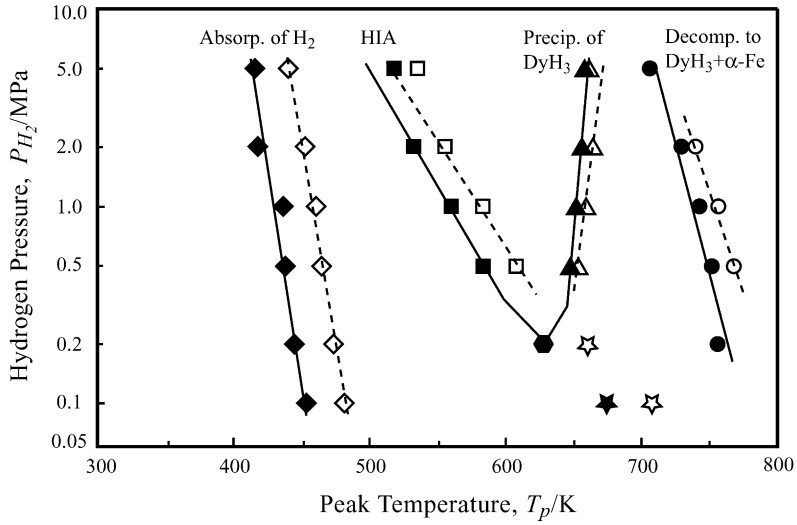

Fig. 9. The relation between the hydrogen pressure and the peak temperatures T_p of the thermal reactions for two heating rates of 0.17 K/s (the solid symbol and the solid line) and 0.33 K/s (the open symbol and the broken line). The solid hexagon denotes that HIA and the precipitation of BiF_3-type DyH_3 occur simultaneously. The pentagrams indicate the direct decomposition of crystalline hydride.

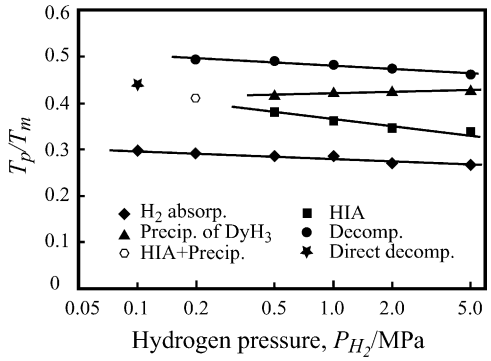

Fig. 10. The relation between the hydrogen pressure and T_p/T_m for the thermal reactions of $DyFe_2$ heated at the rate of 0.17 K/s. Here, T_m is the melting point of $DyFe_2$ (K).

The solid hexagon denotes that HIA and the precipitation of BiF_3-type DyH_3 occur simultaneously and the pentagrams indicate the direct decomposition of the crystalline hydride into α-Fe + DyH_3. As the heating rate increases, T_p shifts to the high temperature side, suggesting the thermally activated process. We focus on the hydrogen pressure dependence of T_p heated at the rate of 0.17 K/s. As the hydrogen pressure increases, T_p for hydrogen absorption, HIA and the decomposition of the remaining amorphous hydride shift to the lower temperature side, but T_p for the precipitation of BiF_3-type DyH_3 shifts to the high temperature side. As a consequence of such pressure dependence, the extrapolated line connecting T_p for HIA intersects the extrapolated line connecting T_p for the precipitation of BiF_3-type DyH_3 at about 640 K and 0.12 MPa H_2. It is expected that HIA and the precipitation of BiF_3-type DyH_3 occur simultaneously at this point. In fact, they occur at a slightly higher pressure, i.e. 0.2 MPa, and a slightly lower temperature, i.e. at 629 K. At the hydrogen pressure below the intersecting point, T_p for HIA is higher than that for the precipitation of BiF_3-type DyH_3, which implies that the amorphous hydride is unstable. Then, the crystalline hydride decomposes directly into α-Fe and BiF_3-type DyH_3 at 0.1 MPa H_2 without the formation of an amorphous hydride.

Fig. 10 shows the relation between the hydrogen pressure and T_p/T_m for the thermal reactions of $DyFe_2$. Here, T_m (K) is the melting point of $DyFe_2$. T_p/T_m for hydrogen absorption is about 0.3 at 0.2 MPa H_2 and is slightly reduced with increasing pressure. T_p/T_m for HIA is 0.38 at 0.5 MPa H_2 and is rapidly reduced to 0.33 at 5.0 MPa H_2. T_p/T_m for the precipitation of BiF_3-type DyH_3 in the amorphous hydride is 0.42 at 0.2 MPa H_2 and is slightly increased to 0.43 at 5.0 MPa H_2. On the other hand, T_p/T_m for the decomposition of the remaining amorphous hydride into α-Fe + DyH_3 is about 0.5 and is slightly reduced with increasing pressure. The pressure dependence of T_p/T_m for the precipitation of BiF_3-type DyH_3 is very strange, because an increasing hydrogen pressure usually enhances the diffusion of H and Dy.

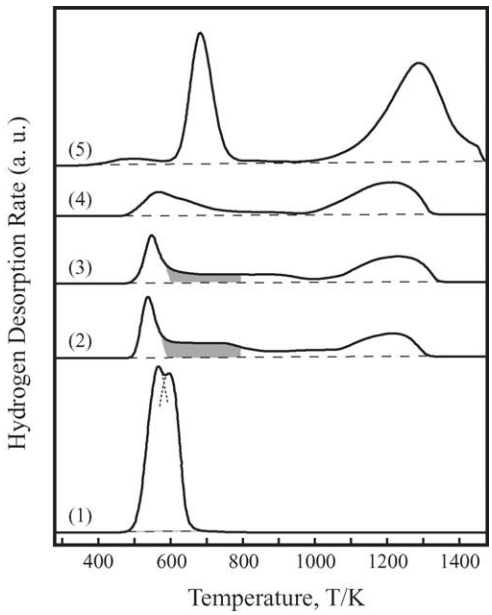

Fig. 11. TDS, heated at the rate of 2 K/s using a hydrogen analyzer in an argon atmosphere, for the samples: (1) c-$DyFe_2H_{4.4}$; (2) a-$DyFe_2H_{3.4}$; (3) a-$Dy_{1-y}Fe_2H_x$ + DyH_3; (4) α-Fe + DyH_3; and (5) for Dy hydride prepared by hydrogenation of pure Dy at room temperature in 5 MPa H_2 for 86 K/s.

3.3. Thermal desorption spectrum (TDS) of hydrogen and the crystal structure of Dy hydride precipitated in the amorphous hydride

Fig. 11 shows TDS, heated at a rate of 2 K/s using a hydrogen analyzer in an argon atmosphere, for the samples: (1) c-$DyFe_2H_{4.4}$; (2) a-$DyFe_2H_{3.4}$; (3) a-$Dy_{1-y}Fe_2H_x$ + DyH_3; (4) α-Fe + DyH_3, which were prepared by thermal analysis of $DyFe_2$ in 1.0 MPa H_2. TDS for (5) the Dy hydride prepared by hydrogenation of pure Dy at room temperature in 5 MPa H_2 for 86 k/s is also shown in this figure. The broken line denotes the base line of TDS. TDS for c-$DyFe_2H_{4.4}$ shows sharp and overlapping peaks at around 500–650 K, which indicates that all of the hydrogen is desorbed from the crystalline hydride and no DyH_3 is formed. On the other hand, TDS for a-$DyFe_2H_{3.4}$ shows a small and sharp peak, at around 500 K, which is gradually weakened with increasing temperature. The small and sharp peak, which is in nearly the same position as the peak of the crystalline hydride, indicates that some of hydrogen in the amorphous hydride is trapped in sites similar to those of the crystalline hydride. The spectra between about 600 and about 800 K (the shadowed part) implies that some of hydrogen atoms are trapped more tightly than those in the crystalline hydride, which is closely related with the driving force of HIA. TDS for this sample shows a broad peak at about 1100–1300 K, which are due to hydrogen desorption from CaF_2-type DyH_2 as discussed later. TDS for a-$Dy_{1-y}Fe_2H_x$ + DyH_3 is similar to that for a-$DyFe_2H_{3.3}$ because of the similarity of chemical compositions of both phases.

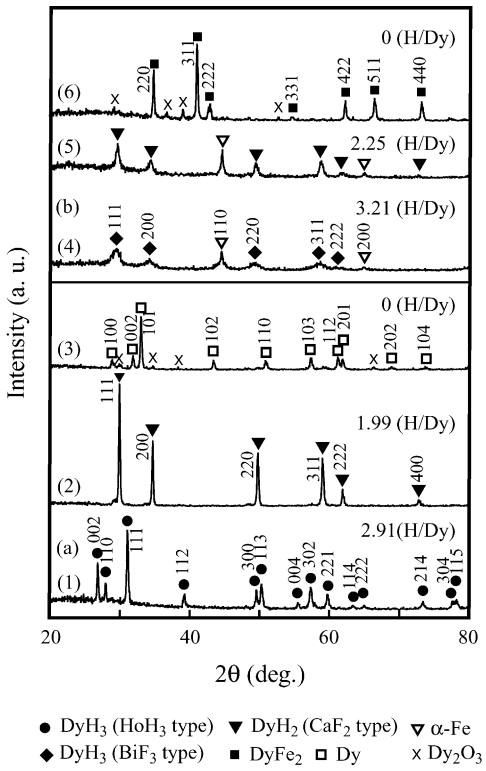

Fig. 12. XRD patterns of (a) Dy hydride prepared by hydrogenation (1) and subsequently heated to 973 K (2), and 1773 K (3) in the hydrogen analyzer and of (b) a mixture of α-Fe + DyH_3 (4) prepared by hydrogenation of the amorphous alloy and subsequently heated to 773 K (5) and to 1373 K (6).

Next, we compare TDS for a mixture of α-Fe + Dy hydride prepared by the decomposition of the amorphous hydride with that for the Dy hydride prepared by hydrogenation at room temperature in 5 MPa H_2 for 86 k/s. TDS for the former sample shows broad peaks at around 500–700 and 1000–1300 K, while the later one shows a sharp and large peak at around 600–750 K and a broad and large peak at around 1100–1400 K.

Fig. 12 shows the XRD patterns of (a) the Dy hydride prepared by hydrogenation of pure Dy and subsequent heating to above the peaks of TDS and of (b) a mixture of α-Fe + Dy hydride prepared by thermal analysis of $DyFe_2$ and subsequent heating to above the peaks of TDS. The hydrogen content (H/Dy) for these samples is also shown in this figure. The XRD pattern of the Dy hydride prepared by hydrogenation of pure Dy is indexed on the basis of HoH_3-type DyH_3. The XRD patterns of this sample after heating to above the first peak (973 K) and to above the second peak (1773 K) of TDS are indexed on the basis of CaF_2-type DyH_2 and pure Dy, respectively. Consequently, the first and the second peak of TDS is due to the transformation from HoH_3-type DyH_3 to CaF_2-type DyH_2 and from CaF_2-type DyH_2 to pure Dy, respectively.

The XRD pattern of a mixture of α-Fe + the Dy hydride prepared by thermal analysis does not substantially change by heating to above the first peak of TDS (973 K), although

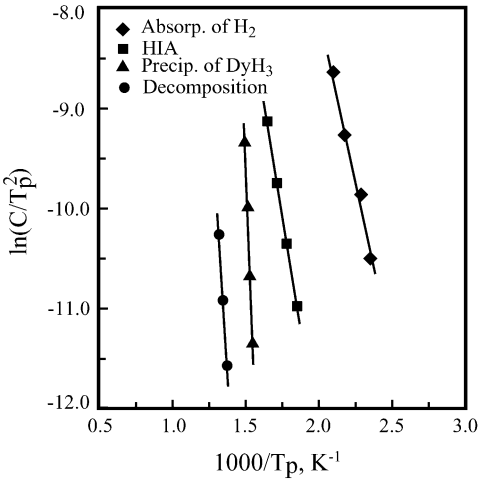

Fig. 13. An example of the Kissinger plot for thermal reactions of $DyFe_2$ heated in 1.0 MPa H_2.

the Bragg peaks of the Dy hydride for the former sample are slightly broadened. However, the hydrogen content decreases from 3.21 to 2.25 (H/Dy). Consequently, the Dy hydride for the former and the latter sample are concluded to be BiF_3-type DyH_3 and CaF_2-type DyH_2, respectively. The XRD pattern of the sample heated to above the second peak of TDS is indexed on the basis of C15 Laves phase $DyFe_2$. Consequently, the first and the second peak in TDS of a mixture sample of α-Fe and the Dy hydride are due to the transformation from BiF_3-type DyH_3 to CaF_2-type DyH_2 and the transformation from CaF_2-type DyH_2 to pure Dy, respectively. The Dy atoms react with α-Fe by the solid state reaction, which gives rise to the formation of the C15 Laves $DyFe_2$.

3.4. The enthalpy change ΔH and the activation energy E_A for the thermal reactions related with hydrogen

The activation energy E_A for the thermal reactions of $DyFe_2$ heated in a hydrogen atmosphere of 1.0 MPa is evaluated by the Kissinger's peak shift method. The method includes the application of the next equation.

$$\ln(C/T_p^2) = -(E_A/RT_p) + A \quad (1)$$

where C is the heating rate, T_p the peak temperature, E_A the activation energy, R the gas constant, and A is a constant. Fig. 13 shows an example of a Kissinger plot for the thermal reactions of $DyFe_2$ heated in 1.0 MPa H_2. From the slope of this straight line, the activation energy E_A is calculated and shown together with the other data in Table 1. On the other hand, the value of the enthalpy change ΔH for the thermal reactions of $DyFe_2$ heated in 1.0 MPa H_2 is calculated from the area of exothermic peaks of PDSC and shown in Table 1.

Fig. 14 shows a schematic illustration of ΔH and E_A for the thermal reactions, heated in: (a) 1.0; and (b) 0.1 MPa H_2 in reaction sequence, in addition to ΔH for the formation of $DyFe_2$. Here, ΔH for hydrogen desorption is plotted to

Table 1
The activation energy E_A and the enthalpy change ΔH of hydrogen absorption, HIA, the precipitation of DyH_3 and the decomposition of the amorphous hydride for $DyFe_2$ heated in 1.0 and 0.1 MPa H_2

	Absorption of H_2	Desorption of H_2	HIA	Precipitation of DyH_3	Decomposition
$DyFe_2$ in 1.0 MPa					
Enthalpy change (kJ/mol Dy)	−53	+6	−27	−7	−9
Activation energy (kJ/mol Dy)	56		75	308	162
$DyFe_2$ in 0.1 MPa					
Enthalpy change (kJ/mol Dy)	−37	+27			−73
Activation energy (kJ/mol Dy)	62				80

the upper direction, because hydrogen desorption occurs endothermically. We can see that E_A for all reactions takes a larger absolute value than that of ΔH when $DyFe_2$ is heated in 1.0 MPa H_2. The activation energy E_A for hydrogen absorption, HIA, the precipitation of BiF_3-type DyH_3 and the decomposition of the amorphous hydride are calculated to

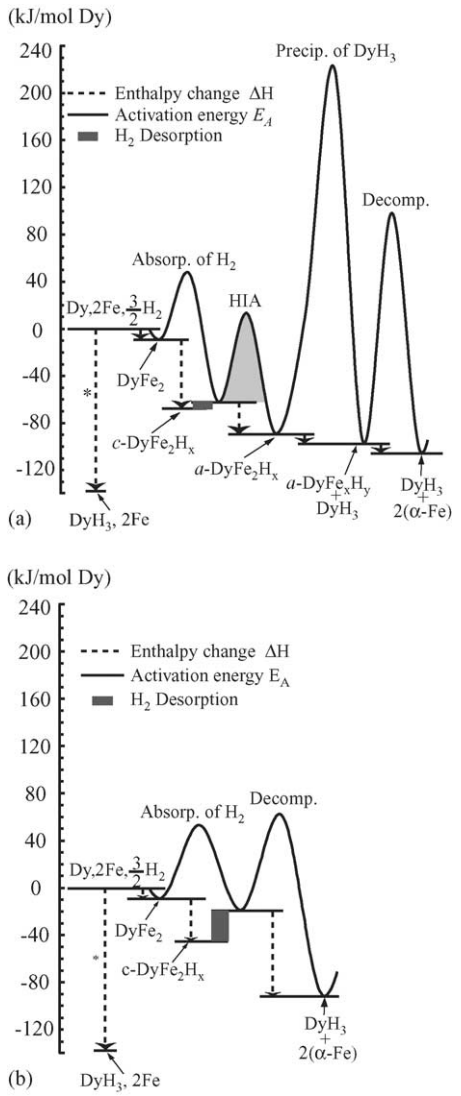

Fig. 14. The value of ΔH and E_A for thermal reactions in the reaction sequence of $DyFe_2$ heated in 1.0 (a) and 0.1 MPa H_2 (b).

be 56, 75, 308 and 162 kJ/mol Dy, respectively, which are closely related with the mechanism of HIA.

According to Hess's Law, ΔH for a reaction is independent of the reaction route. The final products of $DyFe_2$ heated in 1.0 and 0.1 MPa H_2 are α-Fe + DyH_3. Therefore, the total value of ΔH should be equal to that for the formation of DyH_3. A physical mixture of Dy, 2Fe, $3H_2/2$ is the starting point of each reaction and ΔH is 0 here. The formation enthalpy ΔH_f of $DyFe_2$ is calculated to be −9 kJ/mol Dy by the Miedema model [16]. Similarly, the formation enthalpy ΔH_f of DyH_2 and DyH_3 are calculated to be −220 and −138 kJ/mol Dy, respectively. The sums of ΔH for the thermal reactions of $DyFe_2$ heated in 1.0 and 0.1 MPa H_2 are −99 and −92 kJ/mol Dy, respectively. Thus, the sum of ΔH for all thermal reactions in the Dy–Fe–H_2 system is in good agreement with ΔH_f (−138 kJ/mol Dy) of DyH_3. The enthalpy consideration supports the formation of BiF_3-type DyH_3 instead of the formation of CaF_2-type DyH_2.

4. Discussion

4.1. The crystal structure of Dy hydride precipitated in the amorphous phase

The crystal structure of the Dy hydride precipitated in a-$DyFe_2H_x$ and of that formed by the direct decomposition of c-$DyFe_2H_x$ seems at the first glance to be CaF_2-type DyH_2 as shown in Figs. 3 and 6(a and b). However, the hydrogen content of them is 3.2 (H/Dy), so that this hydride should be DyH_3. We discuss the crystal structure of the Dy hydride precipitated in the amorphous hydride. As it is well known, CaF_2-type RH_2 is formed by hydrogenation of rare earth metals R [17]. On the other hand, BiF_3-type RH_3 and HoH_3-type RH_3 are formed by hydrogenation of the light rare earth metals R (La, Ce, Pr and Nd) and of the heavy rare earth metals R (Sm, Gd, Dy, Ho and so on) [18], respectively. It is impossible to distinguish between CaF_2-type hydride RH_2 and BiF_3-type hydride RH_3 by XRD experiments, because the R atoms occupy the same sites in the fcc-type lattice. In CaF_2-type RH_2, the R atoms occupy both face centered and cube corner sites, and the H atoms occupy tetrahedral sites. If the H atoms occupy octahedral sites in addition to the tetrahedral ones, then this is BiF_3-type RH_3. The occupation number of R in the unit cell of the fcc-type lattice is 4, while that of the

tetrahedral and the octahedral sites are 8 and 4, respectively, so that the formula of BiF_3-type hydride is expressed as RH_3.

Next, we discuss why HoH_3-type DyH_3 is not formed, but BiF_3-type DyH_3 is formed by the precipitation and by the decomposition of the amorphous hydride. When CaF_2-type DyH_2 transforms into HoH_3-type DyH_3, large structural changes of the host metal Dy must occur. On the contrary, CaF_2-type DyH_2 transforms into BiF_3-type DyH_3 without a change in the crystal structure of the host metal Dy. CaF_2-type DyH_2 precipitated in a-$DyFe_2H_x$ is surrounded by the amorphous phase, so that its transformation into HoH_3-type DyH_3 is hindered by the amorphous hydride. Consequently, BiF_3-type DyH_3 is formed by the precipitation in the amorphous hydride and by the decomposition of the remaining amorphous hydride.

4.2. The mechanism of hydrogen-induced amorphization

The PDSC curve of $DyFe_2$ heated in 1.0 MPa H_2 shows four exothermic peaks due to: (1) the formation of the crystalline hydride; (2) hydrogen-induced amorphization; (3) the precipitation of BiF_3-type DyH_3; and (4) the decomposition of the remaining amorphous hydride. On the other hand, the curve of the sample heated in 0.2 MPa H_2 shows three exothermic peaks due to: (1) the formation of the crystalline hydride; (2) the simultaneous occurrence of HIA and the precipitation; and (3) the decomposition of the amorphous hydride. Furthermore, the curve of the sample heated in 0.1 MPa H_2 shows only two exothermic peaks due to (1) the formation of the crystalline hydride and the direct decomposition of it into α-Fe + DyH_3. Thus, the thermal reactions of $DyFe_2$ heated in H_2 depend on the hydrogen pressure. We discuss the mechanism of HIA in the C15 Laves phase $DyFe_2$ from the standpoint of the pressure dependence of structural changes. Thermal reactions related with hydrogen are controlled by the kinetic and thermodynamic factors. At about 0.3 T_m, where the diffusion of the metallic atoms does not substantially occur, hydrogen is absorbed forming the crystalline hydride c-$DyFe_2H_x$ without a change in the crystal structure, although a distortion of the crystal lattice occurs. When c-$DyFe_2H_x$ is heated to above the second exothermic peak (583 K), i.e. to about 0.36 T_m, where both Dy and Fe atoms can move over a short-range distance, the transformation from the crystalline to the amorphous hydride, i.e. HIA occurs so as to reduce the enthalpy. The driving force for HIA is considered to be the enthalpy difference resulting from the different hydrogen occupation sites. Hydrogen atoms in c-$DyFe_2H_x$ occupy tetrahedral sites surrounded by 2Dy + 2Fe and Dy + 3Fe by the geometric constraint [19]. The overlapped peak of TDS for c-$DyFe_2H_x$ may correspond to hydrogen desorption from these 2Dy + 2Fe and Dy + 3Fe tetrahedral sites. On the other hand, hydrogen atoms in the amorphous hydride can occupy tetrahedral sites surrounded 4Dy and 3Dy + 1Fe in addition to 2Dy + 2Fe and Dy + 3Fe [20], because there is no geometric constraint for the structure. Since the formation enthalpy of the Dy hydride is more negative than that of the Fe hydride, hydrogen atoms can stay more stable in the amorphous hydride. The small and sharp peak of TDS at around 500 K for a-$DyFe_2H_x$ may correspond to hydrogen desorption from 2Dy + 2Fe and Dy + 3Fe tetrahedral sites. The tailed peak at the higher temperature side of TDS for a-$DyFe_2H_x$ (a shaded part) may correspond to hydrogen desorption from 4Dy and 3Dy + 1Fe tetrahedral sites. As the hydrogen pressure increases, the peak temperature T_p for HIA shifts to the lower temperature side, indicating that H_2 enhances the short-range diffusion of Dy and Fe atoms. BiF_3-type DyH_3 precipitates in the amorphous hydride at about 0.42 T_m. As the hydrogen pressure increases, T_p for the precipitation of BiF_3-type DyH_3 becomes high and shows positive (reverse) pressure dependence. As the hydrogen pressure increases, the diffusion of Dy and hydrogen is generally enhanced which gives rise to a reduction of T_p. Consequently, the precipitation of BiF_3-type DyH_3 may be not controlled by the diffusions of Dy and H_2, but by Fe atoms which do not interact with hydrogen. The decomposition of the remaining amorphous hydride into α-Fe + DyH_3 is controlled by the long-range diffusion of both Fe and Dy atoms, because it occurs at about 0.5 T_m where the long-range diffusion of them become generally more active.

The present work demonstrates that HIA in $DyFe_2$ occurs above a critical hydrogen pressure and below a critical heating rate as shown in Figs. 1 and 2. We discuss the reason why HIA does not occur at low hydrogen pressure. The hydrogen content in the crystalline hydride is 1.48, 1.36 and 1.36 (H/M) for hydrogen pressures of 1.0, 0.2 and 0.1 MPa H_2, respectively. Since there is a little difference in the hydrogen content, it is considered that the occurrence of HIA is not determined by the value of the hydrogen content, but by the hydrogen pressure. As shown in Fig. 9, T_p for HIA shows a strong and negative hydrogen pressure dependence, while that for the precipitation of BiF_3-type DyH_3 shows a weak and positive one. As a consequence of such pressure dependence, HIA overlaps with the precipitation of BiF_3-type DyH_3 in intermediate hydrogen pressure region, while the crystalline hydride decomposes directly into α-Fe and BiF_3-type DyH_3 in low hydrogen pressure. Thus, the pressure dependence of HIA and the precipitation of BiF_3-type DyH_3 play an important role in determining whether HIA occurs or does not occur in $DyFe_2$. The pressure dependence of T_p for HIA may be controlled by short-range diffusion of the Dy and Fe atoms. On the other hand, it is a future subject to determine which atoms control the precipitation of BiF_3-type DyH_3.

5. Summary and conclusion

The pressure dependence of structural changes in the C15 Laves phase $DyFe_2$ heated in a hydrogen atmosphere was investigated by PDSC, XRD, Ar-DSC, TEM and hydrogen analyzer. Four exothermic reactions, i.e. hydrogen absorption in the crystalline state, HIA, the precipitation of BiF_3-type DyH_3 and the decomposition of the remaining amorphous hydride occurred sequentially when $DyFe_2$ was heated at

0.5 MPa H_2 and higher pressures. The second exothermic peak occurs as a result of HIA, the simultaneous occurrence of HIA and the precipitation of DyH_3, and the direct decomposition of amorphous hydride into DyH_3 + α-Fe with decreasing hydrogen pressure. It is the first time that BiF_3-type DyH_3 has been found to precipitate in an amorphous hydride, because the transformation from CaF_2-type DyH_2 into HoH_3-type is restrained by the surrounding amorphous hydride. As the hydrogen pressure increases, the peak temperature of hydrogen absorption, HIA and the decomposition of the remaining amorphous hydride shift to the lower temperature side, but that of precipitation of BiF_3-type DyH_3 shifts slightly to higher temperature side. It is worth noticing that no amorphous hydride is formed at a low hydrogen pressure and at a high heating rate. Furthermore, there is no clear difference in the hydrogen content for the crystalline hydride, when the samples were heated to above the first exothermic peak in 0.1, 0.2 and 1.0 MPa H_2. From these experiment results, we conclude that the controlling factor for HIA in $DyFe_2$ is not the hydrogen content, but the hydrogen pressure which has a close relation with the diffusion of metal atoms.

Acknowledgement

This work was supported in part by a “Grant-in-Aid” for Scientific Research on Priority Area A of “New Protium Function” from the Ministry of Education, Culture, Sports, Science and Technology.

References

[1] X.L. Yeh, K. Samwer, W.L. Johnson, Appl. Phys. Lett. 42 (1983) 242.
[2] K. Aoki, T. Yamamoto, T. Masumoto, Scr. Metal. 21 (1987) 27.
[3] L.E. Rehn, P.R. Okamoto, J. Pearson, R. Bhadra, M. Grimsditch, Phys. Rev. Lett. 59 (1987) 2987.
[4] U.-I. Chung, Y.-G. Lim, J.-Y. Lee, Philos. Mag. B 63 (1991) 1119.
[5] K. Aoki, T. Masumoto, J. Alloys Compd. 231 (1995) 20.
[6] A.Y. Yermakov, N.V. Murshnikov, N.K. Zajkov, V.S. Gaviko, V.A. Barninov, Philos. Magn. B 68 (1993) 883.
[7] K. Aoki, X.G. Li, T. Aihara, T. Masumoto, Mater. Sci. Eng. A 133 (1991) 316.
[8] S. Luo, J.D. Clewley, T.B. Flanagan, Acta Mater. 44 (1996) 4187.
[9] K. Aoki, Mater. Sci. Eng. A 304–306 (2001) 45.
[10] H. Atsumi, M. Hirscher, E.H. Buchler, J. Mossinger, H. Kronmüller, J. Alloys Compd. 231 (1995) 71.
[11] V. Paul-Boncour, S.M. Filipek, A. Percheron-Guegan, I. Marchuk, J. Pielaszek, J. Alloys Compd. 317/318 (2001) 83.
[12] M. Dilixiati, K. Kanda, K. Ishikawa, K. Aoki, Mater. Trans. 43 (2002) 1089.
[13] K. Aoki, K. Mori, T. Masumoto, Mater. Trans. 43 (2002) 2685.
[14] K. Aoki, M. Dilixiati, K. Ishikawa, J. Alloys Compd. 337 (2002) 128.
[15] K. Aoki, M. Dilixiati, K. Ishikawa, Mater. Sci. Eng. A 375–377 (2004) 922.
[16] F.R. de Boer, R. Boom, W.C.M. Mattens, A.R. Miedema, A.K. Niessen, Cohesion Met. (1988).
[17] K.A. Gschneidner Jr., L.R. Eyring, in: Handbook on the Physics and Chemistry of Rare Earth, vol. 3, 1979, p. 309.
[18] M. Mansmann, W.E. Wallace, J. Phys. 25 (1964) 454.
[19] D. Ivey, D. Northwood, J. Less Common Met. 115 (1986) 23.
[20] K. Itoh, K. Kanda, K. Aoki, T. Fukunaga, J. Alloys Compd. 356/357 (2003) 664.